Refilling drug delivery depots through the blood

Yevgeny Brudno[a,b,1], Eduardo A. Silva[a,b,c,1], Cathal J. Kearney[a,b,d], Sarah A. Lewin[a], Alex Miller[b], Kathleen D. Martinick[a], Michael Aizenberg[a], and David J. Mooney[a,b,2]

[a]Wyss Institute for Biologically Inspired Engineering, Harvard University, Boston, MA 02115; [b]School of Engineering and Applied Sciences, Harvard University, Cambridge, MA 02138; [c]Department of Biomedical Engineering, University of California, Davis, CA 95616; and [d]Department of Anatomy, Royal College of Surgeons in Ireland, Dublin 2, Ireland

Edited by Robert Langer, Massachusetts Institute of Technology, Cambridge, MA, and approved July 30, 2014 (received for review July 10, 2014)

Local drug delivery depots have significant clinical utility, but there is currently no noninvasive technique to refill these systems once their payload is exhausted. Inspired by the ability of nanotherapeutics to target specific tissues, we hypothesized that blood-borne drug payloads could be modified to home to and refill hydrogel drug delivery systems. To address this possibility, hydrogels were modified with oligodeoxynucleotides (ODNs) that provide a target for drug payloads in the form of free alginate strands carrying complementary ODNs. Coupling ODNs to alginate strands led to specific binding to complementary-ODN–carrying alginate gels in vitro and to injected gels in vivo. When coupled to a drug payload, sequence-targeted refilling of a delivery depot consisting of intratumor hydrogels completely abrogated tumor growth. These results suggest a new paradigm for nanotherapeutic drug delivery, and this concept is expected to have applications in refilling drug depots in cancer therapy, wound healing, and drug-eluting vascular grafts and stents.

nanoparticle | targeting | DNA nanotechnology | controlled release | biomaterials

Drug-eluting polymer systems have proved useful in a variety of clinical settings, including prevention of restenosis with stenting (1, 2), cancer treatment (3), and enhancing wound healing (4–7). These systems benefit from tunable drug release kinetics, days or even weeks of continuous drug release, and local delivery, which together provide spatiotemporal control over drug availability and can diminish drug toxicity (8). However, existing drug-eluting systems have a finite depot of drug and become unneeded when spent and, in the case of nondegrading systems, may need surgical removal. For many therapeutic applications, an invasive procedure is needed to inject or implant a drug-eluting device, and these devices cannot be refilled or replaced without another invasive surgery.

We propose a new paradigm in drug delivery, the refilling of a delivery device in vivo in a minimally invasive manner, via targeting with fresh drug payloads through the blood. In this paradigm, the injectable delivery device is modified to bind refills infused into the blood (Fig. 1*A*). Drug payloads infused into the blood of a patient extravasate into target tissues and are bound by the device (Fig. 1*B*), subsequently allowing for sustained release of drug at the target site (Fig. 1*C*). One polymer capable of both local controlled drug release and blood-based targeting is alginate, a naturally occurring polysaccharide composed of α-L-guluronic and β-D-mannuronic acid sugar residues (9). Alginate is widely applied in the pharmaceutical industry as an excipient for drugs (10) and as a wound dressing (11). Alginate is biocompatible and nonimmunogenic and can be gelled under gentle conditions, allowing encapsulation of drugs or biological factors with minimal trauma. Additionally, alginate is readily chemically modified for cell adhesion or as a drug carrier (12–14) and has tunable degradation rates (15), and chemically modified forms of alginate are currently used clinically as a drug delivery vehicle for proteins that promote regeneration of mineralized tissue (16) and have been used as a carrier for transplanted cells (14, 17–19). Drug-eluting injectable alginate hydrogels were chosen due to their ability to be introduced into the body in a minimally invasive manner (14). Nanoparticle-sized alginate strands were used for refilling due to their extensive use as modifiable drug carriers (20), and a target site with enhanced permeability (tumors) was chosen to enable passive accumulation of the alginate strands before binding to the target hydrogel (21–23). Together, these elements were used to demonstrate a DNA nanotechnology-based approach for blood-based drug refilling of intratumor drug depots.

Results

Free Alginate Strand Pharmacokinetics. Efficient blood-based refilling of drug payloads relies on a sufficient circulation lifetime to allow payloads to encounter and bind to the primary device. The physical characteristics and pharmacokinetics of free strands of 5% oxidized alginate polymers (alginate strands) were analyzed following bolus i.v. administration in mice through measurement of fluorescence from a near-IR dye stably conjugated to alginate through an amide bond (Fig. S1 *A* and *B*). Previous studies have highlighted that the hydrodynamic radius contributes to the biodistribution and pharmacokinetics of polymers in ways that may not be reflected by the molecular weight (24). Therefore, the hydrodynamic radius of alginate strands was measured by dynamic light scattering (DLS) and gel permeation chromatography (GPC). Oxidized alginate strands showed significantly reduced hydrodynamic radii relative to unoxidized material (15–17 nm vs. 45 nm) despite being of only slightly lower molecular weight (Table S1). Pharmacokinetic analyses (Fig. S1*C*) of oxidized alginate showed that the circulation time for a fraction of the dose was short, with much of the injected dose distributing from the blood 1 min after i.v. injection (Fig. S1*C*), similar to that reported previously for gold nanoparticles (25). The elimination phase for these particles was much slower (half-life for elimination, $\beta t_{1/2}$, ~7.5 h) (Fig. S1*C*), with low levels of strands in the blood through the 48-h course of the pharmacokinetics study. The distribution volume was 0.087 L/kg, and clearance was 1.3 $mL \cdot min^{-1} \cdot kg^{-1}$, in line with previous reports for high

Significance

Drug delivery depots used in the clinic today are single use, with no ability to refill once exhausted of drug. Our system exploits nucleic acid complementarity to refill drug-delivering depots through the blood. The utility of this approach is demonstrated by its ability to inhibit tumor growth to a greater extent than strategies that rely on enhanced permeability and retention alone. We anticipate our approach will be directly applicable to therapies for many diseases, including cancer, wound healing, and inflammation, and for drug reloading of vascular grafts and stents.

Author contributions: Y.B., E.A.S., C.J.K., M.A., and D.J.M. designed research; Y.B., E.A.S., C.J.K., S.A.L., A.M., and K.D.M. performed research; Y.B., E.A.S., C.J.K., S.A.L., A.M., K.D.M., M.A., and D.J.M. analyzed data; and Y.B., M.A., and D.J.M. wrote the paper.

The authors declare no conflict of interest.

This article is a PNAS Direct Submission.

[1]Y.B. and E.A.S. contributed equally to this work.

[2]To whom correspondence should be addressed. Email: mooneyd@seas.harvard.edu.

This article contains supporting information online at www.pnas.org/lookup/suppl/doi:10.1073/pnas.1413027111/-/DCSupplemental.

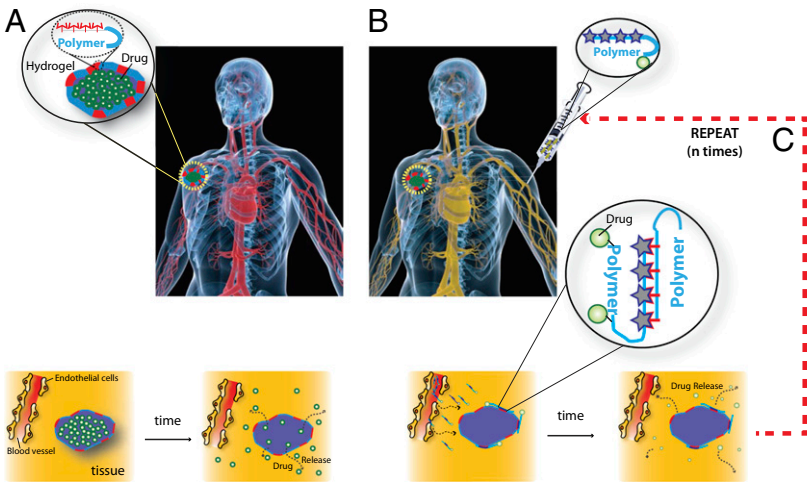

Fig. 1. Schematic for i.v. refilling of drug-delivering devices with therapeutic drugs payloads. (*A*) A drug-delivering device is implanted into a target tissue site and releases active drug (yellow) in a controlled, localized manner. (*B*) i.v. infused drug payloads home to the device site and refill the device with a fresh depot of drug. (*C*) Drug payloads release their cargo in a controlled manner over time. i.v.-mediated drug refilling can be repeated with the same or a different drug payload multiple times.

molecular weight (MW) polymers (26, 27). Tissue distribution at 12 h and 24 h was primarily in the liver and kidneys, with lesser accumulation in the intestines, lungs, spleen, and stomach and very little signal present in the heart and brain (Fig. S2). Little difference was observed between biodistribution at 12 h and 24 h in agreement with previous reports (28–32).

Oligodeoxynucleotide-Mediated Binding of Free Strands to Alginate Gels in Vitro. It was hypothesized that device refilling with drug payloads could be mediated by complementary oligodeoxynucleotide (ODN) binding between target calcium-alginate gel and alginate strands conjugated to a drug payload. ODNs (Table S2 shows a list of ODNs used) were conjugated via their 3′ ends to alginate strands at a ratio of 2 eq ODNs per molecule of alginate (Fig. S3). The ability of alginate-conjugated ODNs to retain nucleic acid binding activity was then tested. Alginate conjugated to $(T)_{20}$ oligonucleotides was ionically cross-linked with calcium to form a gel and then was incubated with fluorescently labeled complementary $(A)_{20}$ or noncomplementary $(T)_{20}$ oligonucleotides (Fig. 2*A*) in phosphate buffer with 1 mM calcium chloride. Complementary oligonucleotides bound to the gel surface in a sequence-specific manner whereas noncomplementary oligonucleotides showed little binding (Fig. 2 *B* and *C*).

The ability of ODN-conjugated alginate gels to bind ODN-conjugated alginate strands was next tested in vitro, as a model for drug refilling in vivo. ODN-conjugated or unconjugated alginate was gelled and incubated with alginate strands coupled to fluorescently labeled complementary ODNs for variable times in a buffer with physiological calcium concentration (Fig. 3*A*). Alginate strands bearing complementary ODNs specifically bound to ODN-bearing gel surfaces, with about fivefold selectivity compared with control gel surfaces; this selectivity was constant over time (Fig. 3 *B* and *C*). To more completely represent a drug-bearing alginate–ODN conjugate, alginate conjugated to ODNs was modified along its backbone with a near-IR dye to mimic drug loading and tested for association with complementary or noncomplementary ODN-bearing alginate gels. Within 30 min of incubation, the fluorescently labeled alginate strands selectively bound to complementary-ODN–bearing gels, compared with control gels bearing noncomplementary ODNs (Fig. 3 *D*–*F*).

In Vivo ODN-Mediated Free Alginate Strand Retention. It was next investigated whether fluorescently labeled alginate strands could home in vivo to a target gel through sequence-mediated targeting. ODNs were conjugated to alginate through the 3′ end to increase serum exonuclease stability (33–35). ODN-conjugated alginate strands were still competent to bind in a sequence-specific manner after 6 h, 12 h, and 24 h of circulation in the blood (Fig. S4).

A melanoma cancer model was chosen for these studies due to the well-established enhanced permeability and retention effect in these tumors (22), which provides a means for passive accumulation of strands in tumor tissue. Mice bearing tumors between 10 mm^3 and 20 mm^3 in size received intratumor injections of ODN-conjugated calcium cross-linked alginate gels. At 24 h,

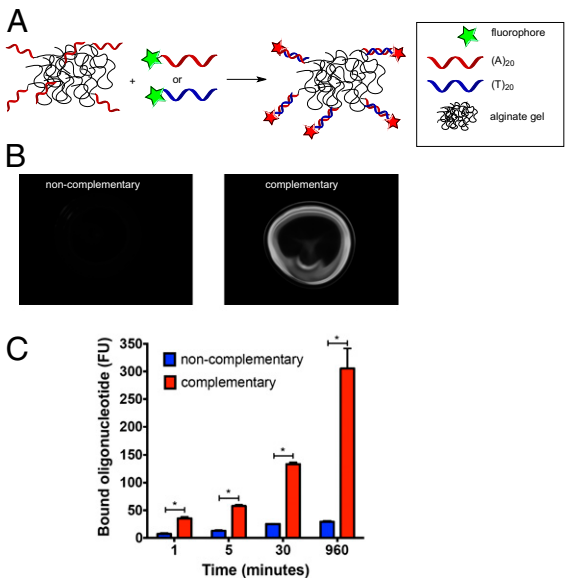

Fig. 2. Sequence-specific binding between ODN-conjugated hydrogels and oligonucleotides. (*A*) Schematic image of ODN-conjugated calcium alginate gels incubated for various time periods with fluorescently labeled complementary or noncomplementary ODN. (*B* and *C*) Fluorescent images after 30 min of incubation (*B*) and quantitation of retained fluorescence on beads after variable incubation times and washing away unbound ODN (*C*). Values represent mean and SEM, $n = 3$. *$P < 0.05$ by Student's t test.

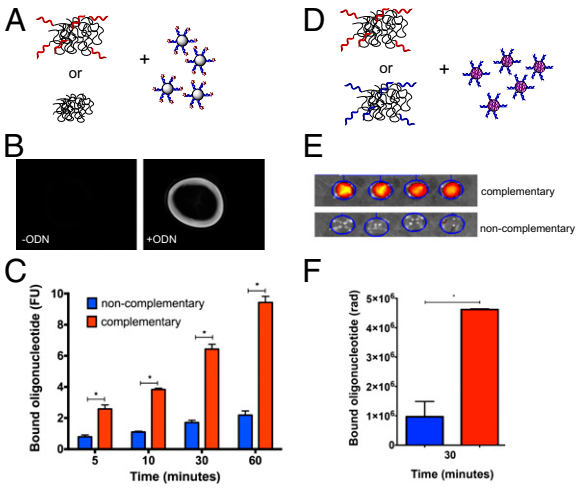

Fig. 3. Sequence-specific binding between ODN-conjugated hydrogels and ODN-conjugated free alginate strands. (*A*) Calcium alginate gels composed of polymer conjugated to ODNs or unconjugated alginate were incubated for various time periods with free alginate strands conjugated to fluorescently labeled complementary ODNs. (*B* and *C*) Fluorescent images after 1 h (*B*) and quantitation of retained fluorescence on gels after incubation for different periods of time and washing away unbound alginate (*C*). (*D*) Calcium alginate gels composed of polymer conjugated to complementary or noncomplementary ODNs were incubated for 30 min with free alginate strands conjugated to ODN and near-IR fluorescent tags. (*E* and *F*) Epifluorescence images (*E*) and quantitation of retained fluorescence on gels after washing away unbound alginate (*F*). Values represent mean and SEM, $n = 3$ (*C*) or 4 (*F*). $^*P < 0.05$ by Student's *t* test. $n = 4$.

fluorescently labeled alginate strands conjugated to complementary ODNs were administered i.v. Imaging of mice first revealed that i.v.-administered alginate strands collected in the tumors of all mice at 24 h postadministration, presumably through the EPR effect (Fig. 4 *A* and *B*). Over the course of 1 wk, mice receiving noncomplementary ODN-conjugated gels or those not injected with gel showed a progressive loss of fluorescence in the tumor, reaching a background level of fluorescence by day 5. In contrast, mice receiving complementary ODN-conjugated gels showed continued accumulation of fluorescence on days 2 and 3 after injection and significant retention of fluorescent alginate in the tumor. Total alginate retention is quantified as the area under the curve (Fig. 4*C*). Sequence-mediated alginate homing produced significantly higher alginate strand retention in the tumor compared with that in controls.

Drug Refilling Slows Tumor Growth. The therapeutic efficacy of this approach was next analyzed by examining the ability of the targeting technology to inhibit tumor growth over several weeks. Drug-delivering alginate hydrogels destined for intratumor injection demonstrated sustained release of doxorubicin over a period of weeks (Fig. S5). To carry i.v.-administered drug payloads, alginate was partially oxidized to introduce aldehyde functional groups, allowing coupling of hydrazine–doxorubicin through a hydrolyzable hydrazone linker (15, 36). Oxidized alginate demonstrated sustained release of doxorubicin (Fig. S6 *A* and *B*) without inhibiting the cytotoxicity of released doxorubicin (Fig. S6*C*).

Immunocompromised mice bearing MDA-MB-231 xenograft tumors were injected intratumor with phosphorothioate ODN-conjugated alginate gels releasing doxorubicin (80 μg per animal) or bolus doxorubicin in PBS. After 2 wk, mice received weekly i.v. administrations of alginate strands conjugated to complementary phosphorothioate ODNs and doxorubicin (120 μg per animal) or bolus doxorubicin (120 μg per animal) as a control (Fig. 5*A*). Targeted drug refilling inhibited tumor growth significantly, compared with treatment with bolus doxorubicin control (Fig. 5*B*). The ability of targeted therapy to reduce tumor size was assessed by monitoring the change in tumor size in the 3 d following each i.v. administration. Tumors shrank after the first two drug-targeted treatments, but continued to grow in mice receiving bolus doxorubicin controls (Fig. 5*C*).

As drug reloading appeared to have significant benefit, we wanted to further confirm that the effect was specific to the interaction of complementary ODN strands in vivo and that differences in doxorubicin pharmacokinetics or release could not account for the effects seen. Specifically, the following additional controls were tested (Table S3): (*i*) intratumoral injections of alginate with encapsulated doxorubicin but no conjugated ODNs, coupled with i.v. administration of DNA-conjugated alginate and hydrazone-linked doxorubicin, and (*ii*) intratumoral injections of alginate gels with encapsulated doxorubicin but no bound ODNs, coupled with i.v. administration of free doxorubicin. The total dose of drug injected directly into the tumor and delivered via i.v. administration was kept constant across all groups, as was the frequency of i.v. administration. After 7 wk of tumor growth, tumors treated with the drug reloading technology were markedly smaller than tumors in any of the control conditions (Fig. 5*D*). Quantification of the tumor sizes confirmed the smaller size of the tumors treated with the drug reloading technology compared with the controls ($P < 0.05$ targeted compared with first two controls, Fig. 5*E*).

Discussion

Here we demonstrate that ODN-conjugated alginate drug payloads can be used for refilling of drug-delivering hydrogels containing the complementary sequence and that this concept can be exploited for tumor treatment. Alginate strands demonstrate efficient distribution to tissues and could be conjugated to ODNs and loaded with drug payloads, making these strands attractive carriers for refilling of a drug delivery depot. Alginate strands conjugated to complementary ODNs were shown to bind to calcium cross-linked alginate gels in vitro and to demonstrate improved retention in tumors in vivo. Finally, ODN-conjugated alginate strands carrying a doxorubicin payload could repeatedly

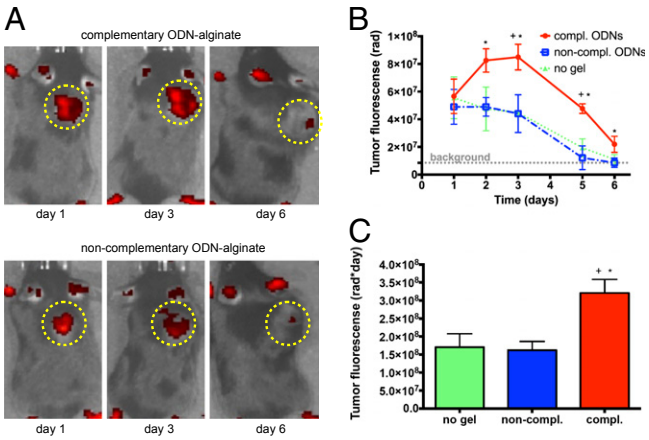

Fig. 4. ODN-mediated refilling of alginate polymers to intratumoral gels. C57/B6 mice bearing B16/F10 melanoma tumors were injected intratumorally with alginate carrying complementary ODNs or noncomplementary ODNs or with no alginate. Retention at the target site was tested through i.v. injection of a fluorescently labeled alginate bearing ODNs. (*A* and *B*) Images (*A*) and quantification (*B*) of fluorescence in the tumor (yellow circles indicate tumor location). (*C*) Alginate residence at the tumor site was quantified by integrating the area under the curve over the 6-day period for each experimental group. Values represent mean and SEM, $n = 4$. $^*P < 0.05$ vs. noncomplementary and $^+P < 0.05$ vs. no gel controls by Student's *t* test.

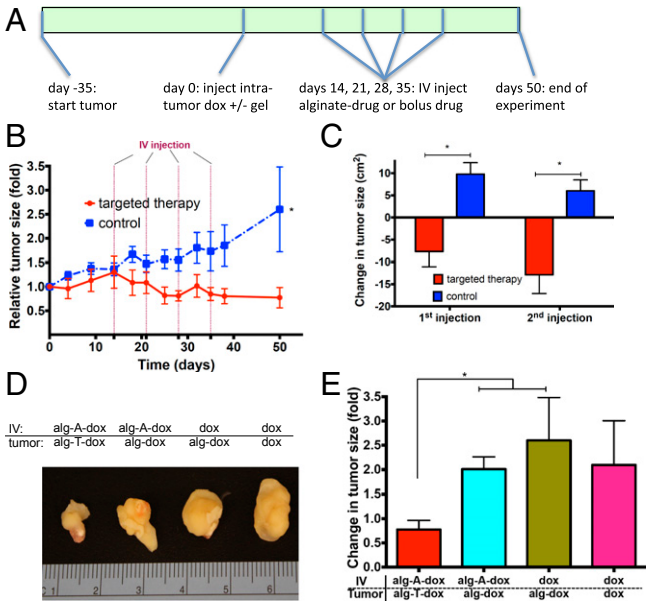

Fig. 5. Drug refilling system leads to arrest in tumor growth in vivo. (*A*) Time frame of experimental design. J:Nu mice were injected with human MDA-MB-231 breast cancer cells at day −35. Tumors were subsequently injected at day 0 with gels conjugated to ODNs, control gels, or PBS with 80 μg doxorubicin. At 2 wk, 3 wk, 4 wk, and 5 wk after gel injection, animals were submitted to i.v. injections of doxorubicin conjugated to alginate and DNA or bolus doxorubicin controls. (*B*) Tumor sizes were monitored over 7 wk after gel injection for targeted and control groups. (*C*) Three-day change in tumor size after each i.v. injection. (*D* and *E*) Photographs of median-sized tumors (*D*) and quantification of tumor growth (*E*) 7 wk after intratumor injection in fully targeted alg-ODN-dox system or control systems with an alg-DNA-dox system incapable of sequence-mediated homing, bolus i.v. injections, or bolus i.v. and intratumor injections. Tumor sizes were normalized to size at day 0. Values represent mean and SEM, $n > 5$. $^*P < 0.05$ by Student's *t* test.

refill an intratumor gel and inhibited tumor growth better than controls reliant on the EPR effect alone.

For efficient homing to target areas, drug payloads must circulate in the blood for sufficiently long periods of time. The results of these studies indicate that the alginate strands remain in circulation for longer than 24 h and the ODNs attached to these particles remain competent to bind to a complementary ODN through at least 12 h. Alginate has previously been reported to have extended circulation times in the blood, being detectable in serum for at least 24 h (37), as well as having PEG-like properties in its ability to increase the circulation time of strands following conjugation (38). The oxidized alginate used in this study had lower viscosity and a lower hydrodynamic radius relative to unoxidized alginate with similar molecular mass (Table S1). The circulation lifetime primarily depends on the rate of excretion into the urine (small molecules), uptake by the mononuclear phagocyte system (MPS) in the liver and spleen (particles), and drug stability. The circulating alginate used in this study had a molecular mass of 200 kDa and a hydrodynamic radius of 15–17 nm. These properties suggest that alginate will behave in these systems, similar to nanoparticles, and will enhance drug circulation time and reduce drug-induced toxicity in off-target tissues. Imaging of individual organs revealed accumulation mainly in the liver, consistent with many nanoparticles, (Fig. S2), and also in the kidneys. Accumulation in the kidneys is likely due to the degradation of the oxidized material over time, releasing smaller alginate particles capable of being filtered by the kidneys.

Nucleic acid complementarity has been widely exploited to direct specific chemical interactions, including controlling chemical reactivity (39, 40), assembly of complex nanostructures (41, 42), surface functionalization (43), and nanoparticle and cell assemblies (44, 45). The utility of nucleic acids in these applications lies in the sequence specificity and strength of binding as well as the tunability of interaction strength. One challenge to this type of application is ODN stability. In this work alginate was conjugated to the 3′ end of ODNs to overcome 3′–5′ exonucleases (the major serum-based nuclease) (33–35) and the backbone was modified with phosphorothioate groups for increased endonuclease and chemical stability (46). These changes were sufficient to protect alginate strand-conjugated ODNs for up to 12 h in circulation (Fig. S4). The stability of the ODN molecules is not unprecedented (47) and may be due to stereochemical protection offered by conjugation to gold nanoparticles and carbon nanotubes (25, 48) or may be due to the high local salt concentrations responsible for improving ODN stability in other polyanionic settings (49).

Drug refilling in the current studies was accomplished via binding of alginate strands to calcium cross-linked alginate gels mediated by complementary sequence interactions. Due to the possibility for nonsequence-mediated interactions in the presence of calcium that could cross-link alginate strands to the gels, in vitro alginate binding studies were performed under a physiologically relevant soluble calcium concentration of 1 mM. Under these conditions, a small amount of alginate does bind to the gels in an ODN-independent manner in vitro (Fig. 3 *C* and *F*). However, ODN-mediated binding of the alginates outpaces nonspecific interactions by fivefold. The significantly increased time that infused alginate remains at the gel site in the in vivo studies also supports the importance of the complementary interaction to at least initially bind the alginate strands to the gels. Whereas studies here were performed with a single set of complementary sequences to refill drug depots, one can imagine taking advantage of multiple sequences to deliver different, orthogonal payloads or take advantage of DNA nanotechnology to create dynamic interactions. Additionally, the scope of drug reloading is not limited to the use of ODNs; other molecular recognition systems such as biotin–streptavidin interactions or "click" chemistries could be used to effect the refilling of drug depots.

Sequence-mediated doxorubicin refilling of alginate gels dramatically inhibited tumor growth in a xenograft tumor model. The breast cancer MDA-MB-231 model was chosen because it is a slow-growing tumor, widely used to test chemotherapeutic strategies (50, 51). Strikingly, the first two refillings of the gel appeared to yield the greatest impact, with a less pronounced effect for the second two refillings. This may be due to degradation of the phosphorothioate oligonucleotides on the gel over the course of the experiment or to saturation of ODN binding sites on the targeted gel. Alternatively, the drug delivery system may have shrunk the tumor to a size in which enhanced permeability was no longer prominent, leading to inefficient targeting. The precise nature of the reduced effect is currently under investigation. Possible degradation could be overcome through the choice of ODNs with improved serum stability such as peptide nucleic acids (52) or mirror-image ODNs (53–55). Saturation of ODNs on the surface of the gels can potentially be overcome through the use of toe-hold exchange technology to remove bound ODNs from the gel to recycle the gel surface for reuse (56).

Because the alginate strands likely cannot penetrate deep into the alginate gels, the number of free strands capable of being bound by the intratumor gels depends, in part, on the surface area of these gels inside the tumor. The injected alginate gels carry a total of $\sim 2 \times 10^{-9}$ mol ODNs, equivalent to the number of strands present in a single i.v. injection. The number of ODNs displayed on the surface of the intratumor gel and able to bind the strands is presumably significantly less than this number. The apparent inability of alginate strands to penetrate deep into the periphery of the gel may account for one limitation of the technology as currently reported. However, the high interstitial pressure (57) inside tumors probably favors the spreading of

injected gel throughout the tumor, increasing the surface area relative to that of a spherical gel and thereby significantly increasing the number of available ODNs on the gel surface. One could also in the future take advantage of injectable macroporous gels and scaffolds (58) to significantly increase both the surface area and the number of ODNs available for free alginate strand binding.

Previous studies have measured EPR-mediated accumulation of nanoparticles and high MW polymers to be ~2–10% /g of tumor (59, 60). The similarity of alginate strands in pharmacokinetics and biodistribution to other high MW molecules suggests that alginate strands likely have similar tumor accumulation. The average tumor size at the time of gel injection was 0.3 g. Therefore, we conservatively estimate that ~1% of i.v.-injected alginate strands accumulate in the tumor due to the EPR effect. The significantly improved retention of fluorescent alginate strands observed in Fig. 4 suggests that the majority of the i.v.-injected alginate strands that accumulate in the tumor are at least transiently bound to the intratumor gels through sequence-specific interactions.

In principle, selective retention of refilling payloads can reduce off-target toxicity at sites such as the liver and areas of wound healing that are currently targeted by any therapy taking advantage of the EPR effect (61–66). The reduced toxicity would occur because increased payload retention at refilled sites and controlled drug release can be combined to reduce overall drug dosing. In addition to direct treatment of tumors, this technology could be used to target tumor sites after biopsy or tumor resection. Alternatively, refilling of drug-eluting devices could be used in other permeable tissues such as occurs during wound healing or at inflammatory sites. Finally, refilling could also aid in delivering drugs to blood-based medical devices such as drug-eluting vascular stents and vascular grafts.

In summary, an ideal system for localized drug delivery would allow for minimally invasive refilling of drug depots for repeat drug dosing over the course of weeks or months. In this study, we have demonstrated a method for blood-based refilling of drug-delivering devices, using nucleic acid sequence complementarity. This proof-of-concept study demonstrates the potential application of refilling other drug-delivery devices in the treatment of many diseases.

Materials and Methods

Material Synthesis. See *SI Materials and Methods* for detailed protocols on ODN synthesis, alginate oxidation and alginate conjugation to ODNs, near-IR dye, and doxorubicin. See Table S4 for chemical properties of alginate polymer used, including MW, viscosity, and hydrodynamic radius.

Doxorubicin Release from Alginate. Doxorubicin or doxorubicin–hydrazide was combined with alginate (oxidized and unoxidized) and gelled with calcium chloride and incubated in PBS at 37 °C. At different time points, the solution was changed and doxorubicin concentrations were measured on a Molecular Devices Spectramax plate reader [excitation (ex) 530 nm, emission (em) 590 nm].

In Vitro Cytotoxicity of Alginate-Coupled Doxorubicin. The cytotoxic effects of hydrazone-linked doxorubicin–alginate and doxorubicin alone were evaluated using the Alamar Blue assay. MDA-MB-231 cells were seeded at a density of 60,000 cells per well in 24-well flat-bottomed plates and incubated for 24 h. Cells were washed twice with PBS and incubated in the culture medium with various concentrations of doxorubicin or alginate-linked doxorubicin for 24 h at 37 °C. Cell viability was evaluated by Alamar blue assay according to vendor instructions and read on a Molecular Devices Spectramax plate reader (ex, 530 nm; em, 590 nm).

Alginate Pharmacokinetic Measurements. Pharmacokinetic studies were performed in CD1 mice and fitted to a two-compartment model, using standard nonlinear analysis. See *SI Materials and Methods* for detailed conditions.

In Vitro Interaction Studies (Fig. 2). Fifteen- to 20-μL droplets of 0.8% unoxidized alginate conjugated to polyA-SH were immersed in a calcium chloride solution (100 mM) for 60 min. Calcium–alginate gels were washed twice with PBS containing 1mM calcium chloride. Five hundred microliters of 0.8 μM fluorescent oligonucleotides (polyT-Fl or polyA-Fl) were added and incubated for 1 min, 5 min, 30 min, or 16 h on an orbital shaker. Samples were washed twice with 500 μL PBS (1 mM $CaCl_2$) and imaged on a fluorescence microscope under the green channel. For quantification, gels were decross-linked in 100 μL 100 mM EDTA for 30 min and fluorescence was read on a Molecular Devices spectramax plate reader (excitation 485, emission 538, cutoff 530).

In Vitro Sequence-Mediated Alginate Binding (Fig. 3 and Fig. S2). Fifteen- to 20-μL droplets of ODN-conjugated alginate (0.5% unoxidized alginate conjugated to polyA-SH or polyT-SH or unconjugated) were immersed in a calcium chloride solution (100 mM) for 60 min. Calcium–alginate gels were washed twice with PBS containing 1 mM calcium chloride. Five hundred microliters of 0.05% alginate conjugated to polyT-SH/HEX (Fig. 3 *A–C*) or to polyA-SH and Dye-750 (Fig. 3 *D–F*) or alginate isolated from blood (Fig. S2) was added and incubated for 5 min, 10 min, 30 min, and 60 min (Fig. 3 *A–C*) or for 30 min (Fig. 3 *D–F* and Fig. S2) on an orbital shaker. Samples were washed twice with 500 μL PBS (1 mM $CaCl_2$) and imaged on a fluorescence microscope (green channel) or on an IVIS Spectrum CT in vivo imager (ex 745 nm, em 820 nm). For quantification, gels were decross-linked in 100 μL 100 mM EDTA for 30 min and fluorescence was read on a Molecular Devices spectramax plate reader.

In Vivo Hydrogel Homing. Animal work was performed in compliance with National Institutes of Health guidelines. All animal experiments were approved by the Institutional Animal Care and Use Committee at Harvard University. Tumors were created by injecting C57/B6 mice s.c. with 100,000 B16-F10 melanoma cells (American Type Culture Collection) in 100 μL PBS in the back of the neck. Animals were monitored for the onset of tumor growth (~2 wk). A total of 20 mg/mL alginate conjugated to ODN (thioT-SH or thioA-SH; see Table S2) was cross-linked with 4% wt/vol $CaSO_4$ (1.22 M) and 50 μL was injected into the center of tumors with a 23-gauge needle. Any covering hair on the tumors was shaved.

One day later, mice were injected retro-orbitally with 100 μL 0.5% ODN-conjugated fluorescent alginate (unoxidized alginate, polyA-SH, Dye-750). Mice were imaged every 24 h for 6 d on an IVIS Spectrum in vivo imager (ex 745 nm, em 820 nm). Mice were euthanized for humane reasons when tumors grew to >20 mm in one direction or when the tumor became ulcerated through skin with a nonhealing open wound present. Mice that died or had to be euthanized before completion of the experiment were not included in the analysis.

Xenograft Tumor Studies. All animal experiments were performed according to established animal protocols. Tumors were created by injecting 10^6 MDA-MB-231 cells (American Type Culture Collection) combined with Matrigel (BD Biosciences) to a total volume of 200 μL (100 μL PBS and 100 μL Matrigel) into the hind limbs of 8-wk-old J:Nu (*Foxn1*^{nu}/*Foxn1*^{nu}) mice (Jackson Laboratories). Thirty-five days following tumor inoculation, tumors were injected with alginate gels. A total of 20 mg/mL alginate conjugated to ODN (thioT-SH or unconjugated) was mixed with doxorubicin (1.6 mg drug per milliliter of gel) and cross-linked with 4% wt/vol $CaSO_4$ (1.22 M), and then 50 μL of gel was injected into tumors with a 23-gauge needle. Two, 3, 4, and 5 wk after initial tumoral gel injection, mice were injected retro-orbitally with 100 μL 0.5% ODN-conjugated alginate carrying doxorubicin [5% oxidized alginate, thioA-SH, Dye-750, 160 μg doxorubicin (Dox)–hydrazide = 120 μg Dox]. Throughout the study, tumor area was measured twice per week with digital calipers in two dimensions and the product of the 2D values was used to approximate tumor area. Mice were killed on day 49. Mice that died or had to be euthanized before completion of the experiment were not included in the analysis.

ACKNOWLEDGMENTS. We are grateful for the assistance of Chris Johnson for help with LCMS and HPLC purification and Dr. Kathleen Pritchett-Corning for help with animal studies. This work was supported by the Wyss Institute for Biologically Inspired Engineering and the National Institutes of Health (R01 EB015498). Y.B. and E.A.S. gratefully acknowledge funding support from the Wyss Technology Development Fellowship. A.M. gratefully acknowledges funding support from the Harvard College Research Program.

1. Simard T, et al. (2014) The evolution of coronary stents: A brief review. *Can J Cardiol* 30(1):35–45.
2. Wessely R (2010) New drug-eluting stent concepts. *Nat Rev Cardiol* 7(4):194–203.
3. Iwamoto T (2013) Clinical application of drug delivery systems in cancer chemotherapy: Review of the efficacy and side effects of approved drugs. *Biol Pharm Bull* 36(5): 715–718.

4. Attanasio S, Snell J (2009) Therapeutic angiogenesis in the management of critical limb ischemia: Current concepts and review. *Cardiol Rev* 17(3):115–120.
5. Freedman SB, Isner JM (2001) Therapeutic angiogenesis for ischemic cardiovascular disease. *J Mol Cell Cardiol* 33(3):379–393.
6. Losordo DW, Dimmeler S (2004) Therapeutic angiogenesis and vasculogenesis for ischemic disease. Part I: Angiogenic cytokines. *Circulation* 109(21):2487–2491.
7. Brudno Y, Ennett-Shepard AB, Chen RR, Aizenberg M, Mooney DJ (2013) Enhancing microvascular formation and vessel maturation through temporal control over multiple pro-angiogenic and pro-maturation factors. *Biomaterials* 34(36):9201–9209.
8. Kearney CJ, Mooney DJ (2013) Macroscale delivery systems for molecular and cellular payloads. *Nat Mater* 12(11):1004–1017.
9. Augst AD, Kong HJ, Mooney DJ (2006) Alginate hydrogels as biomaterials. *Macromol Biosci* 6(8):623–633.
10. Liew CV, Chan LW, Ching AL, Heng PW (2006) Evaluation of sodium alginate as drug release modifier in matrix tablets. *Int J Pharm* 309(1–2):25–37.
11. Matthew IR, Browne RM, Frame JW, Millar BG (1995) Subperiosteal behaviour of alginate and cellulose wound dressing materials. *Biomaterials* 16(4):275–278.
12. Halberstadt C, et al. (2002) A hydrogel material for plastic and reconstructive applications injected into the subcutaneous space of a sheep. *Tissue Eng* 8(2):309–319.
13. Rowley JA, Mooney DJ (2002) Alginate type and RGD density control myoblast phenotype. *J Biomed Mater Res* 60(2):217–223.
14. Silva EA, Kim E-S, Kong HJ, Mooney DJ (2008) Material-based deployment enhances efficacy of endothelial progenitor cells. *Proc Natl Acad Sci USA* 105(38):14347–14352.
15. Bouhadir KH, et al. (2001) Degradation of partially oxidized alginate and its potential application for tissue engineering. *Biotechnol Prog* 17(5):945–950.
16. Bratthall G, et al. (2001) Comparison of ready-to-use EMDOGAIN-gel and EMDOGAIN in patients with chronic adult periodontitis. *J Clin Periodontol* 28(10):923–929.
17. Bent AE, et al. (2001) Treatment of intrinsic sphincter deficiency using autologous ear chondrocytes as a bulking agent. *Neurourol Urodyn* 20(2):157–165.
18. Yu J, et al. (2010) The use of human mesenchymal stem cells encapsulated in RGD modified alginate microspheres in the repair of myocardial infarction in the rat. *Biomaterials* 31(27):7012–7020.
19. Zhao L, Weir MD, Xu HH (2010) An injectable calcium phosphate-alginate hydrogel-umbilical cord mesenchymal stem cell paste for bone tissue engineering. *Biomaterials* 31(25):6502–6510.
20. Brigger I, Dubernet C, Couvreur P (2002) Nanoparticles in cancer therapy and diagnosis. *Adv Drug Deliv Rev* 54(5):631–651.
21. Hiroshi M, Tomohiro S, Toshimitsu K (2001) Mechanism of tumor-targeted delivery of macromolecular drugs, including the EPR effect in solid tumor and clinical overview of the prototype polymeric drug SMANCS. *J Control Release* 74(1–3):47–61.
22. Maeda H, Wu J, Sawa T, Matsumura Y, Hori K (2000) Tumor vascular permeability and the EPR effect in macromolecular therapeutics: A review. *J Control Release* 65(1–2): 271–284.
23. Torchilin V (2011) Tumor delivery of macromolecular drugs based on the EPR effect. *Adv Drug Deliv Rev* 63(3):131–135.
24. Sadekar S, Ray A, Janàt-Amsbury M, Peterson CM, Ghandehari H (2011) Comparative biodistribution of PAMAM dendrimers and HPMA copolymers in ovarian-tumor-bearing mice. *Biomacromolecules* 12(1):88–96.
25. Jensen SA, et al. (2013) Spherical nucleic acid nanoparticle conjugates as an RNAi-based therapy for glioblastoma. *Sci Transl Med* 5(209):ra152.
26. Qhattal HS, Hye T, Alali A, Liu X (2014) Hyaluronan polymer length, grafting density, and surface poly(ethylene glycol) coating influence in vivo circulation and tumor targeting of hyaluronan-grafted liposomes. *ACS Nano* 8(6):5423–5440.
27. Nugent LJ, Jain RK (1984) Two-compartment model for plasma pharmacokinetics in individual blood vessels. *J Pharmacokinet Biopharm* 12(4):451–461.
28. Yu T, Hubbard D, Ray A, Ghandehari H (2012) In vivo biodistribution and pharmacokinetics of silica nanoparticles as a function of geometry, porosity and surface characteristics. *J Control Release* 163(1):46–54.
29. Raghav G, Neha S, Rachana V, Giulio FP, John CB (2009) Biodistribution of TNF-α-coated gold nanoparticles in an in vivo model system. *Nanomedicine* 4(4):401–410.
30. Wang L, et al. (2010) Characterization of gold nanorods in vivo by integrated analytical techniques: Their uptake, retention, and chemical forms. *Anal Bioanal Chem* 396(3):1105–1114.
31. Lee MJ, et al. (2010) Rapid pharmacokinetic and biodistribution studies using cholorotoxin-conjugated iron oxide nanoparticles: A novel non-radioactive method. *PLoS ONE* 5(3):e9536.
32. Park J, et al. (2013) Biodistribution of newly synthesized PHEA-based polymer-coated SPION in Sprague Dawley rats as magnetic resonance contrast agent. *Int J Nanomedicine* 8:4077–4089.
33. Shaw JP, Kent K, Bird J, Fishback J, Froehler B (1991) Modified deoxyoligonucleotides stable to exonuclease degradation in serum. *Nucleic Acids Res* 19(4):747–750.
34. Floege J, et al. (1999) Novel approach to specific growth factor inhibition in vivo: Antagonism of platelet-derived growth factor in glomerulonephritis by aptamers. *Am J Pathol* 154(1):169–179.
35. Gamper HB, et al. (1993) Facile preparation of nuclease resistant 3′ modified oligodeoxynucleotides. *Nucleic Acids Res* 21(1):145–150.
36. Bouhadir KH, Alsberg E, Mooney DJ (2001) Hydrogels for combination delivery of antineoplastic agents. *Biomaterials* 22(19):2625–2633.
37. Al-Shamkhani A, Duncan R (1995) Radioiodination of alginate via covalently-bound tyrosinamide allows monitoring of its fate in vivo. *J Bioact Compat Polym* 10(1):4–13.
38. Kodiyan A, Silva EA, Kim J, Aizenberg M, Mooney DJ (2012) Surface modification with alginate-derived polymers for stable, protein-repellent, long-circulating gold nanoparticles. *ACS Nano* 6(6):4796–4805.
39. Brudno Y, Liu DR (2009) Recent progress toward the templated synthesis and directed evolution of sequence-defined synthetic polymers. *Chem Biol* 16(3):265–276.
40. Yevgeny B, Michael EB, Ralph EK, David RL (2010) An in vitro translation, selection and amplification system for peptide nucleic acids. *Nat Chem Biol* 6(2):148–155.
41. Douglas SM, et al. (2009) Self-assembly of DNA into nanoscale three-dimensional shapes. *Nature* 459(7245):414–418.
42. Wei B, Dai M, Yin P (2012) Complex shapes self-assembled from single-stranded DNA tiles. *Nature* 485(7400):623–626.
43. Onoe H, et al. (2012) Cellular microfabrication: Observing intercellular interactions using lithographically-defined DNA capture sequences. *Langmuir* 28(21):8120–8126.
44. Gartner ZJ, Bertozzi CR (2009) Programmed assembly of 3-dimensional microtissues with defined cellular connectivity. *Proc Natl Acad Sci USA* 106(12):4606–4610.
45. Zhang Y, Lu F, Yager KG, van der Lelie D, Gang O (2013) A general strategy for the DNA-mediated self-assembly of functional nanoparticles into heterogeneous systems. *Nat Nanotechnol* 8(11):865–872.
46. Campbell JM, Bacon TA, Wickstrom E (1990) Oligodeoxynucleoside phosphorothioate stability in subcellular extracts, culture media, sera and cerebrospinal fluid. *J Biochem Biophys Methods* 20(3):259–267.
47. Yu RZ, et al. (1999) Pharmacokinetics and tissue disposition in monkeys of an antisense oligonucleotide inhibitor of Ha-ras encapsulated in stealth liposomes. *Pharm Res* 16(8):1309–1315.
48. Wu Y, Phillips JA, Liu H, Yang R, Tan W (2008) Carbon nanotubes protect DNA strands during cellular delivery. *ACS Nano* 2(10):2023–2028.
49. Seferos DS, Prigodich AE, Giljohann DA, Patel PC, Mirkin CA (2009) Polyvalent DNA nanoparticle conjugates stabilize nucleic acids. *Nano Lett* 9(1):308–311.
50. Choi KY, et al. (2011) Smart nanocarrier based on PEGylated hyaluronic acid for cancer therapy. *ACS Nano* 5(11):8591–8599.
51. Tien J, Truslow JG, Nelson CM (2012) Modulation of invasive phenotype by interstitial pressure-driven convection in aggregates of human breast cancer cells. *PLoS ONE* 7(9): e45191.
52. Demidov VV, et al. (1994) Stability of peptide nucleic acids in human serum and cellular extracts. *Biochem Pharmacol* 48(6):1310–1313.
53. Klussmann S, Nolte A, Bald R, Erdmann VA, Fürste JP (1996) Mirror-image RNA that binds D-adenosine. *Nat Biotechnol* 14(9):1112–1115.
54. Williams KP, et al. (1997) Bioactive and nuclease-resistant L-DNA ligand of vasopressin. *Proc Natl Acad Sci USA* 94(21):11285–11290.
55. Hauser NC, et al. (2006) Utilising the left-helical conformation of L-DNA for analysing different marker types on a single universal microarray platform. *Nucleic Acids Res* 34(18):5101–5111.
56. Zhang DY, Winfree E (2009) Control of DNA strand displacement kinetics using toehold exchange. *J Am Chem Soc* 131(47):17303–17314.
57. Heldin C-HH, Rubin K, Pietras K, Ostman A (2004) High interstitial fluid pressure - an obstacle in cancer therapy. *Nat Rev Cancer* 4(10):806–813.
58. Bencherif SA, et al. (2012) Injectable preformed scaffolds with shape-memory properties. *Proc Natl Acad Sci USA* 109(48):19590–19595.
59. Cabral H, et al. (2011) Accumulation of sub-100 nm polymeric micelles in poorly permeable tumours depends on size. *Nat Nanotechnol* 6(12):815–823.
60. Youichiro N, et al. (1998) Early phase tumor accumulation of macromolecules: A great difference in clearance rate between tumor and normal tissues. *JPN J Cancer Res* 89: 307–314.
61. Park J-H, et al. (2010) Cooperative nanoparticles for tumor detection and photothermally triggered drug delivery. *Adv Mater* 22(8):880–885.
62. Park J-H, et al. (2010) Cooperative nanomaterial system to sensitize, target, and treat tumors. *Proc Natl Acad Sci USA* 107(3):981–986.
63. Ruoslahti E, Bhatia SN, Sailor MJ (2010) Targeting of drugs and nanoparticles to tumors. *J Cell Biol* 188(6):759–768.
64. Simberg D, et al. (2007) Biomimetic amplification of nanoparticle homing to tumors. *Proc Natl Acad Sci USA* 104(3):932–936.
65. von Maltzahn G, et al. (2011) Nanoparticles that communicate in vivo to amplify tumour targeting. *Nat Mater* 10(7):545–552.
66. Perrault SD, Chan WC (2010) In vivo assembly of nanoparticle components to improve targeted cancer imaging. *Proc Natl Acad Sci USA* 107(25):11194–11199.